Molecular Crystals and Liquid Crystals
Publication details, including instructions for authors and subscription information:
http://www.tandfonline.com/loi/gmcl20

Enhancement of Exciton Dissociation Efficiency in Bulk Heterojunction Solar Cells by Using an Intrinsic Photoconductor Component

Upendra K. Pandey [a], Roberto Termine [a], Andreea Ionescu [a], Nicolas Godbert [a], Maria P. De Santo [b], Mauro Ghedini [a] & Attilio Golemme [a]

[a] Centro di Eccelenza CEMIF.CAL, LaSCaMM CR-INSTM della Calabria, CNR-IPCF UOS di Cosenza, Dipartimento di Chimica, Università della Calabria, 87036, Rende, Italy

[b] Physics Department and CNR-IPCF UOS di Cosenza, Università della Calabria, 87036, Rende, Italy

Version of record first published: 18 Apr 2012.

To cite this article: Upendra K. Pandey , Roberto Termine , Andreea Ionescu , Nicolas Godbert , Maria P. De Santo , Mauro Ghedini & Attilio Golemme (2012): Enhancement of Exciton Dissociation Efficiency in Bulk Heterojunction Solar Cells by Using an Intrinsic Photoconductor Component, Molecular Crystals and Liquid Crystals, 558:1, 148-159

To link to this article: http://dx.doi.org/10.1080/15421406.2011.654183

Mol. Cryst. Liq. Cryst., Vol. 558: pp. 148–159, 2012

ISSN: 1542-1406 print/1563-5287 online
DOI: 10.1080/15421406.2011.654183

Enhancement of Exciton Dissociation Efficiency in Bulk Heterojunction Solar Cells by Using an Intrinsic Photoconductor Component

UPENDRA K. PANDEY,[1] ROBERTO TERMINE,[1] ANDREEA IONESCU,[1] NICOLAS GODBERT,[1] MARIA P. DE SANTO,[2] MAURO GHEDINI,[1] AND ATTILIO GOLEMME[1,*]

[1]Centro di Eccelenza CEMIF.CAL, LaSCaMM CR-INSTM della Calabria, CNR-IPCF UOS di Cosenza, Dipartimento di Chimica, Università della Calabria, 87036 Rende, Italy
[2]Physics Department and CNR-IPCF UOS di Cosenza, Università della Calabria, 87036 Rende, Italy

A new type of intrinsic photoconductor was used as a donor in bulk heterojunction solar cells, in blends with PCBM. The donor is a square planar cyclopalladated coordination complex, with a Nile red moiety and a Schiff base as ligands, coordinated by a Pd(II) metal center. The photoconducting properties of the complex were characterized. Photovoltaic devices exhibit low performance, but the analysis of the wavelength dependence of the efficiency reveals a much higher photocurrent upon absorption of the complex, when compared to the photocurrent obtained via absorption by PCBM. This effect is tied to the higher tendency of the intrinsic photoconductor towards exciton dissociation at the heterojunction.

Keywords Organic photovoltaics; bulk heterojunctions; cyclometallated complexes; exciton dissociation

Introduction

The field of organic solar cells has seen considerable developments in the last several years, including improvements in synthesis and fabrication technologies. The potential low cost, flexibility and lightweight make these solar cells promising alternatives to the conventional, silicon based inorganic photovoltaic devices [1–6]. The active layer of the devices usually contains two different phases, either with a bilayer morphology and a single heterojunction, or with bulk heterojunction (BHJ) morphology, where the interface is extended throughout the volume of the active layer. Provided the respective frontier orbital energies are properly tailored, following light absorption excitons diffuse to the heterojunction, where the dissociation of the excitation takes place. When compared to bilayers, BHJ cells combine the advantages of easier fabrication and of higher conversion efficiency due to the considerably extended interface.

*Address correspondence to A. Golemme, Centro di Eccelenza CEMIF.CAL, LaSCaMM CR-INSTM della Calabria, CNR-IPCF UOS di Cosenza, Dipartimento di Chimica, Università della Calabria, 87036 Rende, Italy. E-mail: a.golemme@unical.it

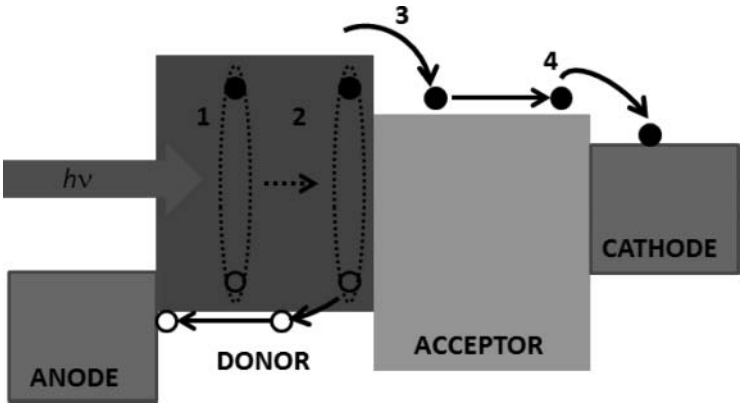

Figure 1. Illustration of the processes leading to photocurrent generation: 1. Photon absorption; 2. Diffusion of exciton towards the donor/acceptor interface; 3. Charge separation; 4. Injection of free charge carriers at the electrodes.

Polymers have often been used in BHJ cells, reaching efficiencies close to 7% [7]. However, they pose several problems related to the control of phase organization, molecular weight polydispersity, and purification. In this context, recent years have seen the emergence of an alternative approach based on the replacement of conjugated polymers by soluble, low molecular weight (LMW) materials [8–12], that present specific advantages in terms of structural definition, synthesis, and purification. In most cases, LMW donors have been developed and used with fullerene $PC_{61}BM$ or $PC_{71}BM$ as acceptors [13–19]. Although their performance still lags behind what can be achieved by using polymers, mainly because of a difficult control of phase morphology, BHJ devices prepared by using only LMW compounds have reached almost a 4% efficiency [20].

The processes involved in current photogeneration are the same in single and bulk heterojunctions. The generation of excitons by photon absorption takes place first. Excitons are bound electron-hole pairs which are difficult to separate at room temperature in the bulk of organic materials. In a second step, these excitons diffuse towards the interface of the donor/acceptor phases. At the heterojunction, excitons separate into free charge carriers (electrons and holes), which drift and diffuse towards the electrodes, where they are collected, entering the external circuit. The different processes of photocurrent generation in an organic solar cell are schematically shown in Fig. 1, where the vertical direction represents electron energy.

Whether polymeric or LMW materials are used, the performance depends then on the same factors, both for single and bulk heterojunctions. Among these, we can mention light absorption, exciton diffusion, efficiency of exciton dissociation at the heterojunction and charge mobility. Although exciton dissociation at the heterojunction is extremely important in determining photocurrents, it is still poorly understood, because of the intrinsic difficulties of both experimental studies and modellizations, and methods for boosting exciton dissociation are needed. The work described in this paper is aimed at establishing the possible improvement in exciton dissociation that can be achieved if the materials used are intrinsic photogenerators, i.e. if they already exhibit a tendency for photogeneration in the bulk, were no interface is present. We present results on BHJ formed by $PC_{61}BM$ and a cyclopalladated Nile Red complex, that belongs to a new class of photoconductors [21]. Although its absorption properties are far from ideal, with obvious consequences on the

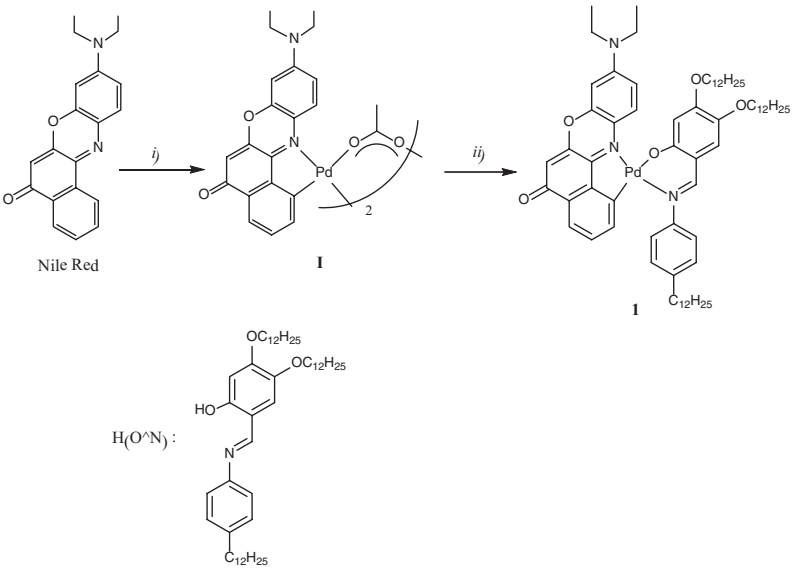

Figure 2. Reagents and Experimental Conditions: i) $Pd(OAc)_2$, Acetic Acid, 55°C, 4 h, ii) H(OˆN), Ethanol, reflux, 2 days.

efficiency, the photoconducting properties of this complex make it a good candidate for testing the effect of intrinsic charge photogeneration on exciton dissociation.

Materials, Samples Preparation and Experimental Methods

The acetato-bridged dimer **I** (see Fig. 2) was synthesised following previously described procedures [22], The Schiff Base **H(OˆN)** was synthesised as described in the following:

4,5-bis(dodecyloxy)-2-hydroxybenzaldehyde [23], (1 g, 2 mmol) and 4-dodecilanilina (0.523 g, 2 mmol) were refluxed in Ethanol (50 mL) for 3h. Upon cooling in an ice bath, a bright yellow precipitate was formed, which was filtered, washed with cold ethanol and dried under vaccum to afford the required **H(OˆN)** Schiff base as a bright yellow crystalline powder.

Yellow solid; yield: 50% (0.741 g); m.p.: 45°C; ^{1}H NMR δ (ppm, $CDCl_3$): 13.67 (s, 1H) 8.45 (s, H_a) 7.21–7.14 (m, 4H) 6.82 (s, 1H) 6.48 (s, 1H) 4.01 (t, J = 7 Hz, 2H) 3.93 (t, J = 7 Hz, 2H) 2.60 (t, J = 8.5 Hz, 2H) 1.89–1.73 (m, 4H) 1.25–1.27 (m, 60H) 0.89–0.84 (m, 9H); E.A. calcd. for $C_{49}H_{83}NO$ (702.15): C 83.81%, H 11.91%, N 1.99%, found C 83.93%, H 11.89%, N 2.02%.

Complex **1** (see Fig. 2) was synthesised as described in the following:

To a solution of **I** (50 mg, 0.05 mmol) in 20 mL ethanol/dichloromethane (1/1 v/v), H(OˆN) (70 mg, 0.1 mmol) was added. The resulting mixture was refluxed overnight and left under stirring at room temperature for another full day. The solvent was evaporated and the resulting dark solid was recrystallized in dichloromethane/methanol to afford **1** as a black crystalline powder.

Black Solid; yield 91% (102 mg); m.p.: 190°C; ^{1}H NMR δ (ppm, $CDCl_3$): 9.33 (d, J = 9.6 Hz, 1H) 7.97 (s, 1H) 7.63–7.59 (m, 2H) 7.33 (s, 1H) 7.20 (s, 1H) 7.15 (s, 1H) 7.12

(s, 1H) 6.81 (t, J = 7.8 Hz, 1H) 6.67–6.69 (m, 2H) 6.50 (d, J = 2.7 Hz, 1H) 6.38 (s, 1H) 6.27 (s, 1H) 6.10 (d, J = 7.2, 1H) 4.01 (t, J = 7.5, 2H) 3.90 (t, J = 7.5 Hz, 2H) 3.55–3.48 (m, 4H) 2.62 (t, J = 7.6 Hz, 2H) 1.84–1.750 (m, 4H) 1.6–1.1 (m, 60 H) 0.88–0.87 (m, 15H); FT-IR (KBr) ν (cm^{-1}): 3449, 2906, 2847, 1700, 1635, 1613, 1580, 1548, 1505, 1403, 1353, 1302, 1281, 1252, 1237, 1212, 1093, 1024, 843, 829, 800, 771, 717, 666; E.A. calcd for $C_{69}H_{99}N_3O_3Pd$ (1124.93), C 73.67%, H 8.87%, N 3.74%, found, C 73.81%, H 8.90%, N 3.73%.

Photo-lithographically patterned ITO glasses (UNAXIS, 110 nm ITO thickness, sheet resistivity 12 Ω/cm^2) were first cleaned in consecutive steps by using distilled water and soap, distilled water, acetone and isopropanol in an ultra-sonicator and were then dried overnight in a vacuum oven at 90°C. Clean substrates were exposed to air plasma (Diener Electronics, Model Femto) for 5 min. The glasses were then spin coated (CaLCTec instruments, Model Fr10KPA-HC) with a 20 nm layer of PEDOT:PSS (Clevios P VP 4081, H. C. Stark GmbH) at 5000 RPM. The PEDOT:PSS coated substrates were then heat treated at 200°C for 10 min on a hot plate to remove any residual solvent. The substrates were immediately transferred inside a nitrogen glove box to avoid any further absorption of water and oxygen by the PEDOT:PSS layer. Solutions of **1**:$PC_{61}BM$ with weight ratios between 1:1 and 1:5 were prepared in chlorobenzene and mixed overnight in the dark. Active layers with thicknesses between 100 to 140 nm were spin-coated at different spinning rates. The samples were then transferred to a thermal evaporator (Kurt J. LESKER) attached to a glove box for the evaporation of the cathode, without exposing them to air. LiF and Al, ~1 nm and 200 nm thick, respectively, were then thermally evaporated at a base pressure of 1.2×10^{-7} mbar. The thicknesses of the different layers of the devices were measured by using a Dektak 8 surface profilometer. The active area of the sample was 8.75 mm^2.

Absorption measurements in solution were performed with a Perkin Elmer 900 UV-Vis spectrometer using normal incidence. Absorption on thin films were performed using a reflection technique. In this case, the incident light from a light source (Oriel, Model 66902) was first directed through a monochromator (Oriel, Model 74100) before reaching the sample at an angle of ~45°. The reflected light was then collected using a power meter (Ophir, NOMA II). This experiment was repeated for a blank in order to calculate the absorption at different wavelengths.

Photoconductivity measurements were performed, using a He-Ne laser (Melles Griot) as a light source, with a Keithley 6517A source meter. For such measurements, two ITO substrates were glued together using spacers with thickness between 1.7 and 5 μm and the samples were then filled by capillarity on a hot plate.

Atomic Force Microscopy (AFM, Bruker Nanoscope IIIa) has been used in the tapping mode. A home-made set up allows to detect shifts in the phase angle of vibration when the oscillating tip interacts with the sample surface. In this work, phase shift images are presented.

Current/voltage characteristics were measured (Keithley 2400 Source Meter) inside a N_2 glove box under simulated solar illumination (Sciencetech, Model SS150 solar simulator, Air Mass 1.5G, 100 mW/cm^2). The solar simulator intensity was tuned by using a calibrated Si photodiode (Hamamatsu S2386-44K).

From the J/V curves it is possible to extract the efficiency of devices. The power conversion efficiency η is defined by

$$\eta = FF\frac{J_{SC}V_{OC}}{I} \quad (1)$$

Where I is light intensity, Jsc is the measured short circuit current density, V_{oc} is the open circuit voltage and FF is the fill factor. FF is defined considering the maximum power P_{max} (obtained from characteristic curves) as:

$$FF = \frac{P_{max}}{J_{OC}V_{OC}} \tag{2}$$

The external quantum efficiency (EQE) is defined by the ratio between the number of charges N_e extracted at the electrode and the total number of photons N_{ph} incident on the device at a particular wavelength as:

$$EQE(\lambda) = \frac{N_e}{N_{ph}} \tag{3}$$

In the experiment, the EQE(λ) was obtained by first measuring the photocurrent density of a calibrated Si photodiode J_{Si} and then the photocurrent density of the device J_D. EQE was calculated as:

$$EQE(\lambda) = QE_{Si}\frac{J_{Si}}{J_D} \tag{4}$$

where QE_{Si} is the quantum efficiency of the calibrated Si photodiode. The internal quantum efficiency IQE was obtained as:

$$IQE(\lambda) = \frac{EQE(\lambda)}{\alpha d} \tag{5}$$

where α is the extinction coefficient of a device of thickness d.

Results and Discussion

The cyclopalladated complex **1** was synthesised through a two steps procedure which involves the formation, by reaction of Nile Red with $Pd(OAc)_2$, of the acetato-bridged dimer **I**, [22], followed by its rupture upon addition of the Schiff base ligand, as illustrated in Fig. 2.

The required Schiff base **H(OˆN)** has been quantitatively obtained by condensation of 4-dodecylaniline with 4,5-bis(dodecyloxy)-2-hydroxybenzaldehyde in refluxed ethanol, following previously reported procedures [23].

Complex **1** belongs to a new class of semiconductors [21], coordination complexes in which the HOMO is positioned on the ancillary Schiff base and the LUMO on the cyclometallated ligand, both coordinated by either a Pt(II) or a Pd(II) metal atom, as shown in Fig. 3.

It is believed that this physical separation is at the origin of the intrinsic charge photogeneration properties of these materials. However, the HOMO/LUMO separation is also important for another reason. In fact, the proper choice of ligands is an easily accessible method for tuning absorption wavelengths. Complex **1** was chosen because, when compared to other compounds of the same class (see Fig. 4) it exhibits an extended absorption range, up to λ ∼650 nm, which is desirable for photovoltaic applications. In addition, the presence of long alkyl chains improves processability during spin coating.

As in the case of other complexes of the same class [24–27], complex **1** is also a photoconductor. Photoconductivity measurements were carried out both on pure **1** and on samples doped with less than 1% of C_{60}. As it is evident from the results illustrated in

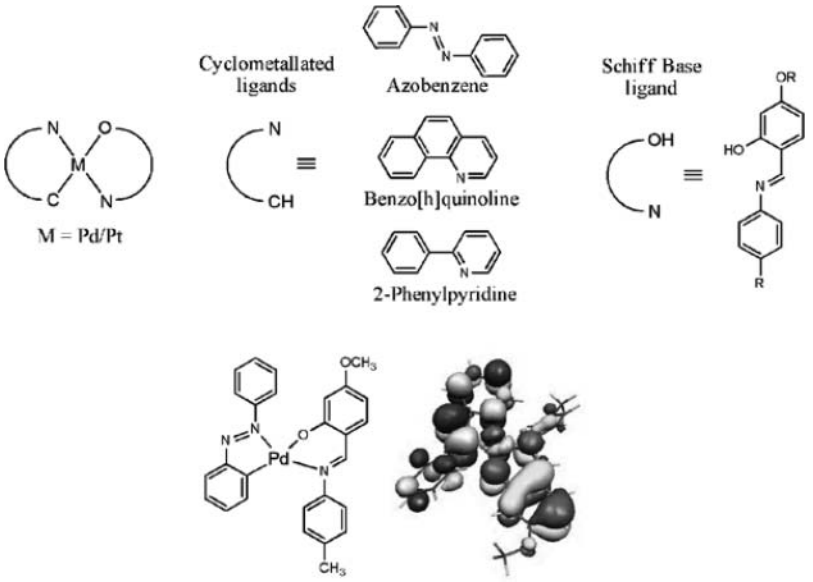

Figure 3. Above: general chemical structure of photoconductive cyclometallated complexes. Below: chemical structure in the case of the azobenzene complex, with HOMO (in green/yellow) and LUMO (in white/blue) distribution.

Fig. 5, the photoconductivity increases by two orders of magnitude in the presence of C_{60}, without a measurable increase in absorption. Since C_{60} is a well known electron acceptor, such increase in photoconductivity shows that i) there is a significant electron transfer from the excited state of **1** to C_{60} and ii) complex 1 is a hole conductor, as already known for the other complexes of the same class [21]. On the basis of these observations, the use of **1** in BHJ devices, in combination with soluble derivatives of C_{60}, seemed possible.

The most common soluble commercial C_{60} compound that plays the role of acceptor in BHJ is $PC_{61}BM$, which was used, in combination with **1**, to obtain BHJ photovoltaic cells, as described in the experimental section. The chemical structure of $PC_{61}BM$ is shown in Fig. 6, together with a schematic diagram of the energy level alignment of frontier orbitals

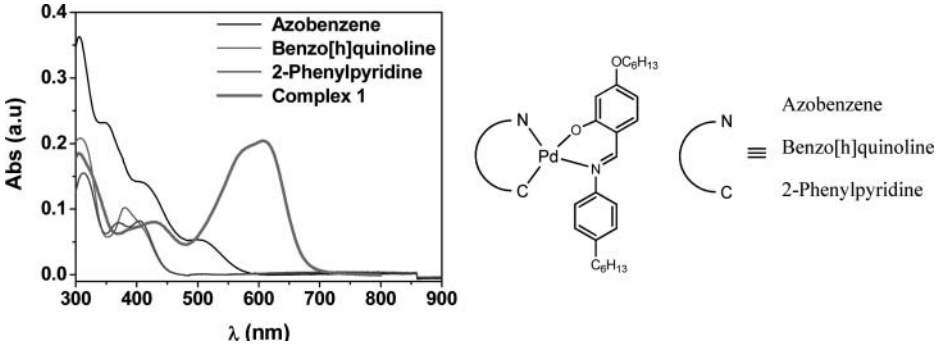

Figure 4. Comparison between the absorption of complex **1** and of other cyclometallated complexes of the same class.

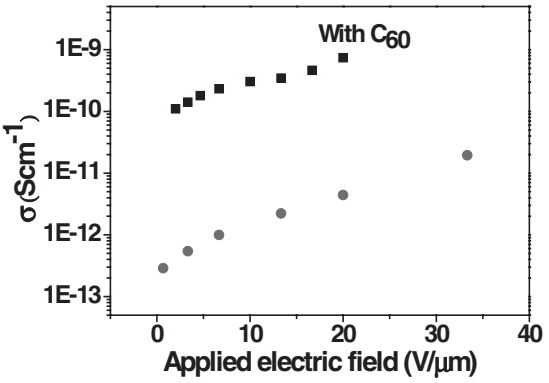

Figure 5. Photoconductivity of pure complex **1** and of complex **1** doped with C_{60} as a function of the applied electric field. The measurements were carried out at $\lambda = 633$ nm, with a light intensity $I = 0.65$ W/cm^2.

for the donor (**1**), the acceptor ($PC_{61}BM$), the PEDOT:PSS hole injection layer and the work functions of the electrodes within the cells.

It is well known that in BHJ solar cells, performance is strongly affected by the morphology of the interpenetrating phases, which, in turn, depends on both the solvent and the composition [28]. BHJ cells were prepared as mentioned in the experimental section by using different solvents, such as dichloromethane, chloroform and chlorobenzene. The best performing solvent was chlrobenzene and only results obtained by using such solvent will be illustrated in the following.

Typical J-V curves in the dark and under illumination are shown in Fig. 7 for the **1**:$PC_{61}BM$ weight ratio 1:4, which gave the best results.

The various parameters of the devices with different compositions are summarized in Table 1. With a 1:1 composition, cells were shorted and it was not possible to perform measurements. It is evident from Table 1 that as the concentration of $PC_{61}BM$ is increased Jsc increases, which is the main reason leading to a higher efficiency, whereas all the other

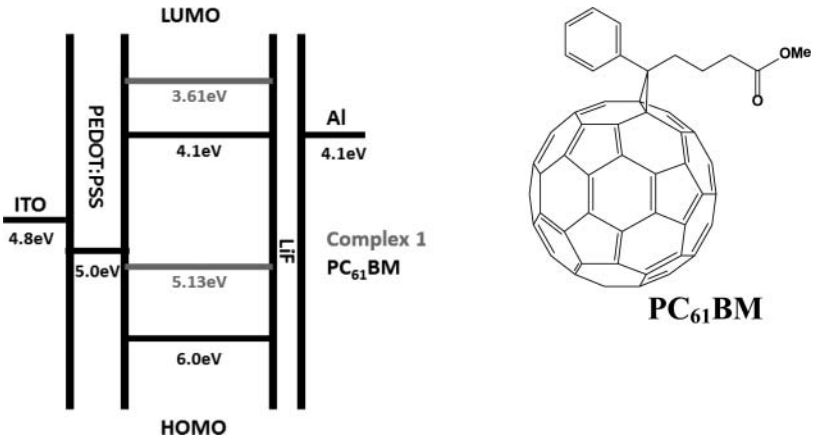

Figure 6. Schematic illustration of the energy levels alignment of the materials used in the devices. The chemical structure of $PC_{61}BM$ is also shown.

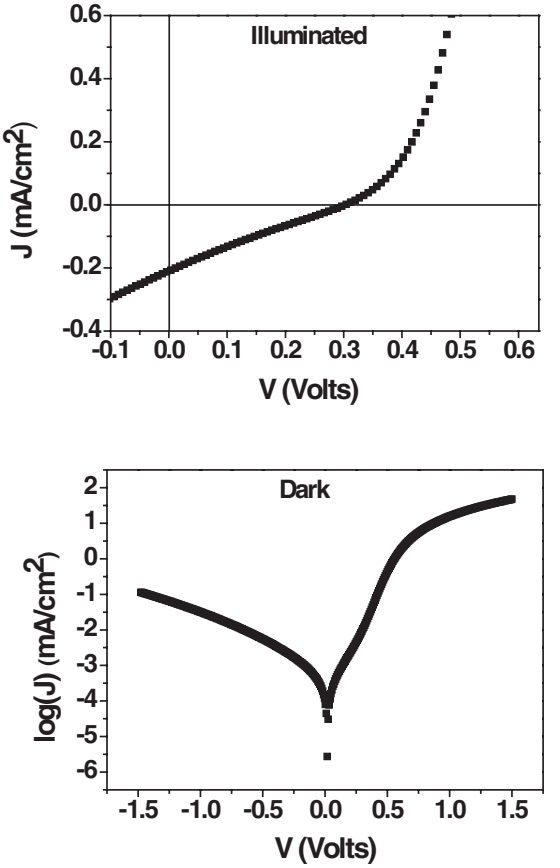

Figure 7. Typical J-V curves for the **1**:$PC_{61}BM$ system with a 1:4 weight ratio, under 100 mW/cm^2 light illumination (AM 1.5) and in the dark.

parameters remains almost constant and independent from composition. However, when the content of complex **1** becomes too low (1:5 composition) the efficiency decreases.

An explanation for the improved performance at higher $PC_{61}BM$ concentration can be found by considering the atomic force microscopy (AFM) images obtained in the phase mode and shown in Fig. 8.

Table 1. Typical parameters of devices at different compositions of the active layer

1:$PC_{61}BM$ Weight Ratio	Jsc (mA/cm^2)	Voc (Volts)	Efficiency	Fill Factor
1:2	0.017	0.24	0.001	0.25
1:3	0.035	0.34	0.003	0.26
1:4	0.195	0.30	0.014	0.24
1:5	0.06	0.35	0.005	0.25

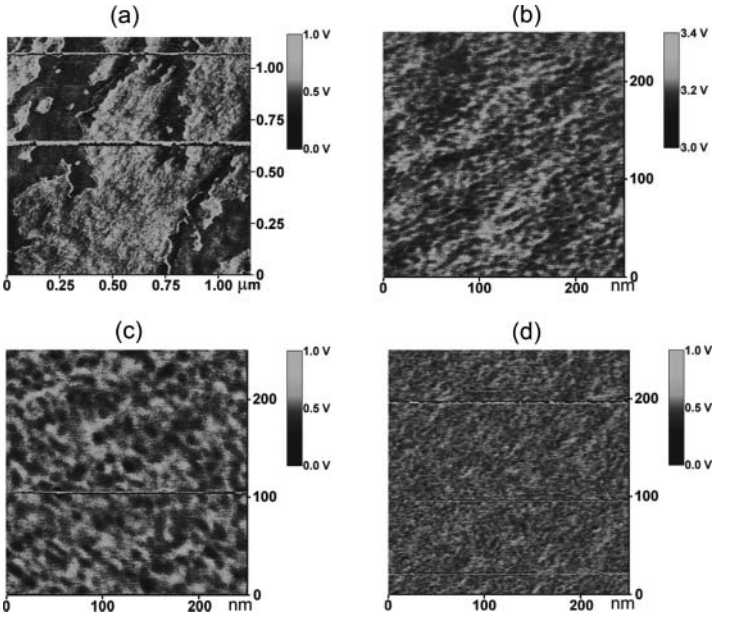

Figure 8. AFM phase images of the **1**:$PC_{61}BM$ active blend with weight ratios 1:1 (a), 1:2 (b), 1:3 (c) and 1:4 (d).

For a 1:1 composition, large patches of the two phases with dimensions of several hundred nanometers can be observed. As the $PC_{61}BM$ concentration is increased, the morphology evolves towards an interpenetrated network, with typical dimensions of the domains ∼25 nm for the 1:3 composition and ∼10 nm for the 1:4 composition. A better performance in BHJ with well connected domains in this size range is expected, because it induces a higher current photogeneration and reduces the series resistance [29]. However, even for the best samples, efficiency is rather low, by roughly two orders of magnitude when compared to the best performing materials in BHJ [7]. One of the possible reasons for this low performance can be found in the difficulty in obtaining a good morphology of the interpenetrating phases in the BHJ, which is typical in devices using LMW materials. Thermal annealing, often used in order to improve morphology [30], was also performed on our samples, at 70°C and 120°C, but it did not lead to an improvement of the efficiency, that actually decreased, indicating that the morphology of the active layer becomes even worse after thermal treatments.

Another reason for the low performance is the low absorption of **1**, which is more than one order of magnitude lower than what would be required for good efficiency. The absorption of a film with a 1:4 composition is shown in Fig. 9. Even at the peak for λ ∼600 nm the absorption coefficient is $\alpha < 10^4\ cm^{-1}$, corresponding to an absorption of less than 20% of the incident photons in a 100 nm thick device.

Despite the low performance, a deeper level of analysis of the data can be interesting in assessing the importance of using a photoconducting component in organic photovoltaic devices. The external and internal quantum efficiencies of a device with a 1:4 composition is shown in Fig. 10.

As expected, EQE follows absorption rather well, except for a shift of the efficiency towards higher wavelengths, but what is more revealing is the wavelength dependence of IQE. It is evident that at higher wavelengths, where the contribution of **1** to absorption is

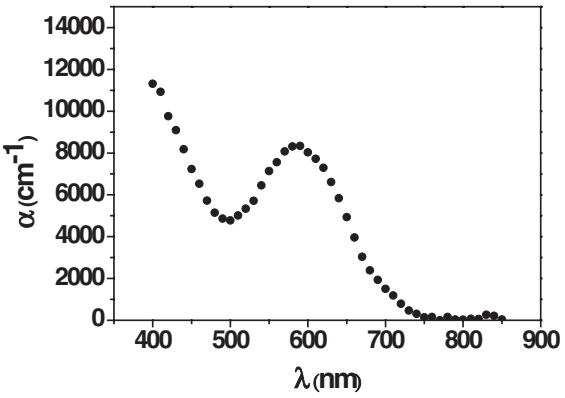

Figure 9. Absorption of a sample with a **1**:$PC_{61}BM$ = 1:4 weight ratio.

higher, higher values of IQE are observed. There is a monotonic decrease of IQE throughout the visible region (data below 750 nm, where the absorption of the devices is very low, are greatly affected by error and are not shown). In other words, light absorbed at higher wavelengths is more effective in generating photocurrent. Although IQE dependences on wavelength reported in the literature are never flat, in this case the behaviour is rather unusual, with IQE varying by a factor 6 between $\lambda \sim$400 nm and $\lambda \sim$750 nm.

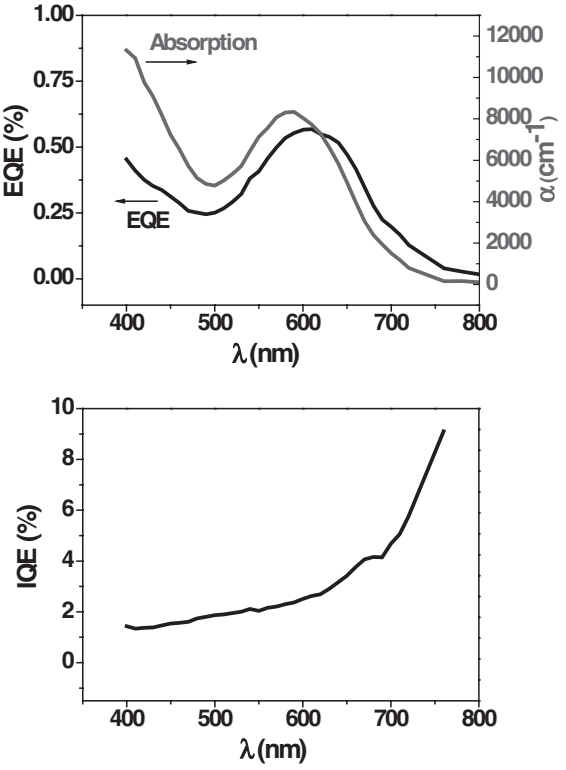

Figure 10. (a) Wavelength dependence of external quantum efficiency and absorption in a film of 1:$PC_{61}BM$ with a 1:4 composition. (b) Internal quantum efficiency of the same film.

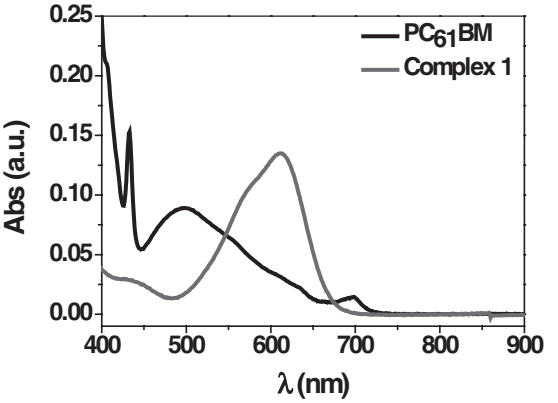

Figure 11. Absorption in solution of Complex **1** and of $PC_{61}BM$.

In order to rationalize this observation it is necessary to consider the relative contribution to light absorption of the two components of the active layer, as shown in Fig. 11.

Complex **1** exhibits an absorption maximum at $\lambda \sim 600$ nm, with an absorption edge at $\lambda \sim 700$ nm and residual absorption up to $\lambda \sim 800$ nm. Absorption decreases at wavelengths below $\lambda \sim 600$ nm, but not dramatically. $PC_{61}BM$ instead shows very little light absorption at high wavelengths, with an extinction coefficient almost monotonically increasing as the wavelength decreases. Simplifying, and considering that $PC_{61}BM$ is much more abundant in the films, we can say that at high wavelengths the contribution to absorption is due mainly to complex **1** and, as the wavelength is decreased, the contribution of $PC_{61}BM$ becomes more and more important. Note how the IQE curve is roughly shaped like the mirror image of the absorption curve for $PC_{61}BM$.

It is clear from the wavelength dependence of quantum efficiency that light absorption by complex **1** leads to a much higher photon-to-collected-charge conversion than absorption by $PC_{61}BM$. The comparison between experiments carried out with different relative concentrations of the components do not show a decrease of the effect when the size of the domains decreases, ruling out the hypothesis that the different performance of the two components could be due to different exciton diffusion lengths of the two materials. Similarly, the contribution of "hot excitons" [31], can be excluded, as the higher conversions are obtained for higher wavelengths. Results can instead be explained by considering the intrinsic photogeneration properties of complex **1**. The tendency of **1** towards charge photogeneration even in the bulk, could be the explanation for the easy charge transfer to $PC_{61}BM$, when compared to other donors. In contrast, absorption by $PC_{61}BM$ is less efficient. In addition, given the fact that complex **1** is an intrinsic photoconductor, a contribution to charge photogeneration far from the interface could also be important. In other words, the thickness of the interface which is relevant for exciton dissociation might not be reduced to a single layer of molecules when the exciton is produced in the complex **1** side of the heterojunction.

Further studies are needed in order to better understand the process and to clarify the underlying mechanisms. However, the data presented in this paper clearly show an unusual behaviour that, at least in the case of the compounds studied, indicates that the use of a photoconductor as a component of excitonic solar cells can dramatically affect exciton dissociation efficiency.

Acknowledgments

The authors thank Dr A. Pane for collaboration in sample preparation in the clean room facility of the IPCF-CNR Lycryl Laboratory.

References

[1] Brabec, C. J., Sariciftci, N. S., & Hummelen, J. C. (2001). *Adv. Funct. Mater.*, *11*, 15.
[2] Peumans, P., Yakimov, A., & Forrest, S. R. (2003). *J. Appl. Phys.*, *93*, 3693.
[3] Dennler, G., Scharber, M. C., & Brabec, C. J. (2009). *Adv. Mater.*, *21*, 1323.
[4] Peet, J., Senatore, M. L., & Heeger, A. J. (2009). *Adv. Mater.*, *21*, 1521.
[5] Brabec, C. J. (2004). *Sol. Energy Mater. Sol. Cells*, *83*, 273.
[6] Wang, D. H., Choi, D. G., Park, O. O., & Park, J. H. (2010). *J. Mater. Chem.*, *20*, 4910.
[7] Chen, H. Y., Hou, J., Zhang, S., Liang, Y., Yang, G., Yang, Y., Yu, L., Wu, Y., & Li, G. (2009). *Nat. Photonics*, *3*, 649.
[8] Silvestri, F., Marrocchi, A., Seri, M., Kim, C., Marks, T. J., Facchetti, A., & Taticchi, A. (2010). *J. Am. Chem. Soc.*, *132*, 6108.
[9] Leriche, P., Frere, P., Cravino, A., Aleveque, O., & Roncali, J. J. (2007). *Org. Chem.*, *72*, 8332.
[10] Zhang, J., Yang, Y., He, C., He, Y., Zhao, G., & Li, Y. (2009). *Macromolecules*, *42*, 7619.
[11] Walkar, B., Kim, C., & Nguyen, T. Q. (2011). *Chem. Mater.*, *23*, 470.
[12] Tamayo, A. B., Dang, X. D., Walker, B., Seo, J. H., Kent, T., & Nguyen, T. Q. (2009). *Appl. Phys. Lett.*, *94*, 103301.
[13] Karpe, S., Cravino, A., Frere, P., Allain, M., Mabon, G., & Roncali, J. (2007). *Adv. Funct. Mater.*, *17*, 1163.
[14] Kopidakis, N., Mitchell, W. J., Lagemaat, J., Ginley, D. S., Rumbles, G., Shaheen, S., & Rance, W. L. (2006). *Appl. Phys. Lett.*, *89*, 103524.
[15] Ma, C. Q., Fonrodona, M., Schikora, M. C., Wienk, M. M., Janssen, R. A. J., & Baurle, P.(2008). *Adv. Funct. Mater.*, *18*, 3323.
[16] Winzenberg, K. N., Kemppinen, P., Fanchini, G., Bown, M., Collis, G. E., Forsyth, C., Hegedus, K., Singh, T. B., & Watkins, S. E. (2009). *Chem. Mater.*, *21*, 5701.
[17] Zhang, J., Yang, Y., He, C., He, Y., Zhao, G., & Li, Y. (2009). *Macromolecules*, *42*, 7619.
[18] Yang, Y., Zhang, J., Zhou, Y., Zhao, G., He, C., Li, Y., Andersson, M., Inganas, O., & Zhang, F. J. (2010). *Phys. Chem. C*, *114*, 3701.
[19] Liu, Y., Wan, X., Yin, B., Zhou, J., Long, G., Yin, S., & Chen, Y. J. (2010). *Mater. Chem.*, *20*, 2464.
[20] Walker, B., Tamayo, A. B., Dang, X. D., Zalar, P., Seo, J. H., Garcia, A., Tantiwiwat, M., & Nguyen, T. Q. (2009). *Adv. Funct. Mater.*, *19*, 3063.
[21] Ghedini, M., Golemme, A., Aiello, I., Godbert, N., Termine, R., Crispini, A., La Deda, M., Lelj, F., Amati, M., & Belviso, S. (2011). *J. Mater. Chem.*, *21*, 13434.
[22] Aiello, I., Ghedini, M., & La Deda, M. (2002). *J. Lumin.*, *96*, 249.
[23] Godbert, N., Dattilo, D., Termine, R., Aiello, I., Bellusci, A., Crispini, A., Golemme, A., & Ghedini, M. (2009). *Chem. Asian. J.*, *4*, 1141.
[24] Aiello, I., Dattilo, D., Ghedini, M., & Golemme, A. (2001). *J. Am. Chem. Soc.*, *123*, 5598.
[25] Termine, R., Aiello, I., Dattilo, D., Ghedini, M., & Golemme, A. (2003). *Adv. Mater.*, *15*, 723.
[26] Ghedini, M., Aiello, I., Crispini, A., Golemme, A., La Deda, M., & Pucci, D. (2006). *Coord. Chem. Rev.*, *250*, 1373.
[27] Cook, S., Ohkita, H., Kim, Y., Benson-Smith, J. J., Bradley, D. D. C., & Durrant, J. R. (2007). *Chem. Phy. Lett.*, *445*, 276.
[28] Wanzhu, C., Ming, W., Jie, Z., Ergang, W., Tingbing, Y., Chao, H., Ji, S. M., Hongbin, W., Xiong, G., & Yong C. J. (2011). *Phys. Chem. C*, *115*, 2314.
[29] Kim, S., Kim, B., & Kim, J. (2010). *Appl. Mater. Inter.*, *6*, 1264.
[30] Verploegen, E., Mondal, R., Bettinger, C., Sok, S., Toney, M., & Bao, Z. (2010). *Adv. Funct. Mater.*, *20*, 3519.
[31] Dennler, G., Forberich, K., Scharber, M. C., & Barbec, C. J. (2007). *J. Appl. Phys.*, *102*, 054516.